Final Draft
of the original manuscript:

Wang, L.C.; Zhong, Y.; Widmann, D.; Weissmueller, J.; Behm, R.J.:
Oxygen Adsorption and Low-Temperature CO Oxidation on a Nanoporous Au Catalyst: Reaction Mechanism and Foreign Metal Effects
In: Topics in Catalysis (2018) Springer Science

DOI: 10.1007/s11244-017-0881-2

Oxygen adsorption and low-temperature CO oxidation on a nanoporous Au catalyst: Reaction mechanism and foreign metal effects

L.C. Wang[1,a], Y. Zhong[2], D. Widmann[1], J. Weissmüller[2,3], R.J. Behm[1]*

[1]Institute of Surface Chemistry and Catalysis, Ulm University, D-89069 Ulm, Germany

[2]Institute of Materials Research, Helmholtz Center Geesthacht,

D-21502 Geesthacht, Germany

[3]Institute of Materials Physics and Technology, TU Hamburg-Harburg,

D-21073 Hamburg, Germany

Abstract

To further our understanding of the role of trace impurities of the second metal in the catalytic performance of unsupported, nanoporous Au (NPG) catalysts, in particular for the activation of O_2, we have prepared a NPG catalyst by electrochemical leaching of Cu from a AuCu alloy and investigated its behavior in the CO oxidation reaction. The structural and chemical properties of the as-prepared catalyst as well as that after reaction for 1000 min were characterized by scanning electron microscopy (SEM), X-ray diffraction (XRD) and X-ray photoelectron spectroscopy (XPS). The nature of the surface oxygen species and the oxygen storage capacity (OSC) were investigated and quantified by multi-pulse experiments in a temporal analysis of products (TAP) reactor. The catalytic behavior in the low-temperature CO oxidation reaction was evaluated both in a TAP reactor under dynamic vacuum conditions and in a conventional micro-reactor under atmospheric pressure. We discuss implications of these results and of similar data obtained previously on a Ag-containing NPG catalyst on the reaction mechanism and on the role of the second metal in the reaction and its impact on the reaction characteristics.

Keywords: Nanoporous Au (NPG) catalyst, CO oxidation, Kinetics, Oxygen storage capacity (OSC), Dynamic studies, Temporal analysis of products (TAP), AuCu alloy

Submitted to Top. Catal.: 25.09.2017

[a] pres. address: Biological and Chemical Processing Department, Idaho National Laboratory, Idaho Falls, Idaho, 83401, USA

* Author to whom correspondence should be addressed, Email: juergen.behm@uni-ulm.de

1. Introduction

In the past few decades, the excellent catalytic activities of nanosized gold have stimulated extensive research activities to elucidate the physical origin for this as well as for exploring its applications for various chemical transformations [1-4]. For low temperature CO oxidation on supported gold catalysts, the catalytic role of gold itself is usually convoluted with the influence of the support materials, in particular for reducible metal oxides [1-4]. More recently, a new class of unsupported nanoporous gold (NPG) catalysts with a ligament size of typically tens of nanometers has been reported to have up to comparable Au mass specific activities as its supported counterparts for CO oxidation under the same reaction conditions [5-9]. The NPG catalysts also exhibit a remarkably high activity and/or selectivity for many other reactions including the preferential oxidation of CO [10;11], the oxygen-assisted coupling of alcohols [12-14], methanol electro-oxidation [15;16], selective hydrogenation of unsaturated aldehydes [17;18] etc.. Ideally, the absence of support materials in the NPG catalysts and of the related interface regions provides the opportunity to examine the intrinsic catalytic properties of gold alone. Nevertheless, residual impurities existing in this type of materials and their potential influence on the catalytic activity has made the presumption of 'pure gold catalyst' questionable and therefore requires careful examination.

The NPG materials are usually prepared by selective leaching or etching of the less noble metals, typically Ag [5-7;12;19], from the corresponding Au alloys. Because of the Ag residues ($\geq$ 1 at.%) in the as-prepared samples, which cannot be completely removed by de-alloying, the nature of the active sites on the Ag-containing NPG catalysts for the low-temperature CO oxidation is still under debate [7;9;11;20-28]. Some researchers have suggested that the high catalytic activity of NPG is attributed to a high density of under-coordinated sites or defects such as atomic steps and kinks resulting from the high curvature of the internal surface of NPG materials [22;23]. The surface density of these defect sites on

NPG is estimated to be comparable to that of 3-5 nm Au nanoparticles [22;23]. Similarly, a recent work suggested that the 6-fold coordinated sites created by twinning defects in the fcc lattice of NPG prepared by dealloying Al_2Au can significantly contribute to the catalytic activity towards CO oxidation [9;27;28]. Other studies indicated, however, that the residual Ag plays a critical role in the oxidation reactions [7;11;20;21;24-26;29]. Accordingly, pure gold was found to show an extremely low activity for activating molecular O_2 for stable oxygen adsorption, which was related to a lower concentration of low-coordination surface active sites compared to small gold particles [30].

To examine the role of Ag in the catalytic activity of NPG, we have investigated the CO oxidation behavior of a series of Ag-containing NPG catalysts (denoted as NPG(Ag) hereafter) with different Ag contents [21]. Our results have unambiguously shown that there is an almost linear correlation between surface Ag concentration and the catalytic activity of the NPG catalysts in the low-temperature CO oxidation reaction [21]. Alternatively, one can compare the catalytic properties of a NPG(Ag) catalyst with a NPG catalyst containing a different residual less-noble metal, such as Cu, with a similar surface area and (surface) Cu composition as present in the NPG(Ag) catalysts. Preliminary results of such measurements, which were published previously [31], revealed a clear influence of the surface content of residual Cu species on both O_2 adsorption and catalytic activity, similar to the role of Ag in the NPG(Ag) catalysts.

Aiming at a more detailed understanding of the role of surface Cu species and the active oxygen species / reaction pathway over NPG(Cu) catalysts, we have continued these studies. In the present paper, we report results of a combined micro-reactor and temporal analysis of products (TAP) reactor study on the kinetics and transient reaction behavior of CO oxidation over a NPG(Cu) sample. First we briefly describe the experimental setup and procedures (section 2). The as-prepared sample was characterized by scanning electron microscopy

(SEM), powder X-ray diffraction (XRD) and X-ray photoelectron spectroscopy (XPS) (section 3.1). The capability of the NPG(Cu) catalyst to activate O_2 for stable oxygen adsorption and to accumulate these active oxygen species (oxygen storage capacity - OSC) was determined by CO titration experiments performed in a TAP reactor after exposure of the samples to either O_2 pulses or to an O_2/N_2 gas flow at atmospheric pressure (section 3.2). These measurements were performed both on the fresh NPG samples (before reaction) and on samples exposed to CO oxidation under atmospheric pressure for 1000 min. The CO oxidation activities of the catalysts were examined in the TAP reactor under vacuum conditions and in conventional micro-reactor measurements at atmospheric pressure (section 3.3). SEM and XRD measurements on the NPG catalyst, performed after the reaction measurements, gained further insight into the structural stability of the NPG(Cu) catalysts. The results obtained on the NPG(Cu) catalyst are compared with those obtained for one of the reported NPG(Ag) catalysts and the implications on the physical origin for the catalytic activity of NPG materials are discussed (section 3.4).

2. Experimental

2.1. Nanoporous gold sample preparation

As described previously [31;32], the Cu-containing nanoporous gold sample was prepared by electrochemical etching (dealloying) of a $Au_{25}Cu_{75}$ (at.%) alloy, which was produced by arc melting of high purity Au and Cu wires (Au 99.995% and Cu 99.99%, Chempur). Following the subsequent homogenization at 900°C for 4 days (sealed in a quartz tube), the alloy was quenched in water. The ingot was rolled to 0.2 mm thickness and annealed at 600°C for 2 h in vacuum for recovery. Dealloying was performed in 1 M $HClO_4$ aqueous solution at a potential of 1.1 V with respect to a Ag/AgCl reference electrode, which was placed directly in the 1 M $HClO_4$ electrolyte close to the sample, for approximately one day. The electrolyte was freshly prepared from 18.2 MΩ cm water and 70% $HClO_4$ (Suprapur®, Merck KGaA). To minimize

copper contamination in the sample compartment, the coiled-Ag wire counter electrode (CE) and the reference electrode (RE) were separated from the main cell by placing them in a tube filled with the same solution and mounted with its opening close to the sample. Dealloying was stopped when the current fell to 10 μA and below. Subsequently, the cell was repeatedly rinsed with deionized water to remove traces of Cu ions in solution. The NPG(Cu) disks were crushed and gently ground into powder before use.

2.2. Catalyst characterization

The surface area of the as-prepared NPG(Cu) material was determined via the capacitance ratio method [33], yielding a value of 49 m^2 g^{-1}. The surface area of the NPG(Cu) sample after reaction (α) was estimated to be 9 m^2 g^{-1} by assuming idealized, cylindrical ligaments with diameter D (the average crystallite size from X-ray diffraction (XRD) results) via the relation $\alpha = 4/\rho D$ [34], where ρ is the mass density of gold (19.32 g cm^{-3}). Note that applying this procedure the surface area before reaction was estimated to be around 60 m^2 g^{-1}, which is close to that measured by the capacitance ratio method (49 m^2 g^{-1}). XRD measurements were performed on a PANalytical MPD PRO instrument, using Cu-Ka radiation (λ = 0.154 nm). The average crystallite sizes were calculated from the Au(111) diffraction peaks by using the Scherrer equation $D = K \lambda / \beta \cos\theta$, where K = 0.89 is the Scherrer's constant, λ the wave length of the X-rays and β the FWHM. Note that this is an empirical relation, we will use the term *apparent ligament size* for the value derived from $D_{Scherrer}$, and use this for the characterization of samples after the catalytic reaction, which cannot be characterized by the capacitance ratio method.

The surface morphology, microstructure and the Cu bulk concentration of the resulting samples were determined by scanning electron microscopy (SEM) and energy dispersive X-ray spectroscopy (EDX), respectively. X-ray photoelectron spectroscopy (XPS) data were

recorded on a PHI 5800 ESCA system (Physical Electronics) using monochromatic Al-K_α radiation. The binding energies of Au(4f) and Cu(2p) were calibrated with reference to the standard C(1s) peak (284.6 eV). The Au and Cu surface concentrations were calculated from the measured intensities of the Au(4f) and Cu(2p) signals using tabulated sensitivity factors, respectively, which assumes a constant composition of the topmost few layers.

2.3 Catalytic activities measured in the flow reactor

The catalytic activity of the NPG(Cu) catalyst for CO oxidation was measured in a micro-reactor with a length of 300 mm and an inner diameter of 4 mm at atmospheric pressure at temperatures of 30 - 150°C, without applying any pretreatment prior to the measurements. The catalyst was diluted with α-Al_2O_3 in order to obtain differential reaction conditions, resulting in conversions of below 15% of the reactants during the catalytic measurements. The temperature of the catalyst bed is measured by a thermal couple attached to the outer wall of the reactor, centered along the catalyst bed. The flow rate of reactant gas was 60 Nml min^{-1} (1% CO, 1% O_2, rest N_2), and both influent and effluent gases were analyzed by on-line gas chromatography (Chrompack CP9001). For further details on the set-up and the evaluation see refs. [35;36].

2.4 TAP reactor measurements

The pulse experiments were carried out in a home-built TAP reactor [37], which is largely based on the TAP-2 approach of Gleaves et al. [38]. In short, piezo-electric pulse valves were used to generate gas pulses of typically ~1×10^{16} molecules per pulse. For all measurements presented, these pulses contained 50% Ar as an internal standard to enable quantitative evaluation on an absolute scale. The gas pulses were directed into a quartz tube micro-reactor with a length of 90 mm and an inner diameter of 4 mm. The catalyst bed was located in its central part and was fixed by two stainless steel sieves (Haver & Boecker OHG, transmission

25%). For all measurements, we used a three-zone catalyst bed containing 2 mg of NPG(Cu) catalyst diluted with 20 mg SiO_2 as central zone and two layers of SiO_2 as outer zones (total mass 150 mg), except for the simultaneous pulse experiment in Fig. 7, where only 0.6 mg Au was used. All pulse experiments were performed at 30°C reaction temperature to lower the temperature-induced ligament growth during reaction [6;19]. Also here, the catalyst was used as received, with no additional pre-treatment prior to the measurements. After passing through the reactor, the gas pulses are analyzed by a quadrupole mass spectrometer (QMG 700, Pfeiffer) located behind the reactor tube in the analysis chamber. The consumption of CO and O_2 in the respective pulses was calculated from the missing mass spectrometric intensity in the pulses compared to the intensity after saturation, which is equivalent to the initial intensity. The formation of CO_2 could be determined directly from the CO_2 pulse intensity. The reactor can be separated from the ultrahigh vacuum (UHV) system by a differentially pumped gate valve and connected directly to an adjustable roughing pump.

The ability of the NPG(Cu) catalyst for active oxygen adsorption, given by the amount of stable adsorbed active oxygen that can be reversibly deposited from interaction with O_2 and reacted away by CO pulses (oxygen storage capacity – OSC), was determined by multi-pulse experiments performed at 30°C. In these measurements, the fresh catalyst was first reduced by a sequence of CO/Ar pulses, until the CO_2 formation was below the detection limit. Subsequently, the catalyst was exposed either to a sequence of O_2/Ar pulses or to a continuous flow of 10% O_2/N_2 with a gas flow of 20 NmL min^{-1} at atmospheric pressure (at 30°C). Then the amount of stable adsorbed oxygen species active for CO oxidation was titrated by a sequence of CO/Ar pulses under vacuum conditions. Since the oxygen uptake was too little to be evaluated directly from the missing intensity in the O_2 pulses, we determined this from the total CO_2 formation during the CO/Ar pulses. The process of oxygen deposition and reactive removal by CO was repeated at least three times for each case in order

to check the reversibility of the active oxygen formation. To examine the catalytic activity in the TAP reactor, the samples were exposed to simultaneous pulses of CO/Ar and O_2/Ar. For both measurements, the resulting CO:O_2 ratio was 1:1 and, hence, there was an excess of oxygen relative to stoichiometric reaction conditions. The measurements with simultaneous pulses were used for comparison with the catalytic activity measured in the micro-reactor. Prior to these measurements it was checked that the gas mixing unit and the gas pipes containing the reaction mixture as well as the reactor and the dilution materials were inert, no conversion of CO or O_2 was found under these conditions in control experiments.

To identify oxygen species present on the surface before and after the reaction, we also performed temperature programmed desorption (TPD) measurements in the TAP reactor. The measurements started directly after reaction, heating the catalyst from 30°C to 600°C with a heating rate of 25°C min^{-1}. The gaseous desorption / decomposition products were transported by diffusion into the analysis chamber, where the effluent gases were detected by the mass spectrometer.

3. Results and Discussion

3.1 Characterization of the NPG(Cu) catalyst

The as-prepared NPG(Cu) sample shows a sponge-like morphology with ligament diameters of below 10 nm (Fig. 1a). Severe coarsening of the porous structure occurred after exposure to CO oxidation reaction mixtures at 30ºC for 1000 min (Fig. 1b). This coarsening of the catalyst structure is further confirmed by XRD measurements, which show a significant sharpening of the Au diffraction peaks after reaction (see Fig. 2). No diffraction peaks characteristic of Cu-containing phases (metallic copper or copper oxides) could be detected in the samples, neither before nor after reaction. Using the Scherrer equation and assuming that the ligaments are single-crystalline, the apparent ligament sizes of the sample NPG(Cu) were determined to be

3.4 and 22 nm before and after reaction (Table 1), respectively. Note that lattice defects / lattice strain could also contribute to the width of the diffraction peaks and the defect structure of the NPG material [39;40] which may not be neglected especially for the fresh sample. Nevertheless, the broadening of the XRD profiles may still be used as an indicator of structure size, assuming that the width of the Bragg reflections indicates a low crystalline coherence on a length-scale in the order of $D_{Scherrer}$. A reaction-induced coarsening of NPG catalyst in CO oxidation has also been observed on the Ag-containing NPG samples that were derived from AuAg alloys in our previous study [21] and also by Xu et al. [19].

The Au(4f) spectra recorded on the fresh NPG(Cu) sample (see Fig. 3a) clearly indicate the existence of Au^{3+} (Au_2O_3) species, reflected by a second peak at a BE of 85.9 eV, which accounts for ~38% of the total Au(4f) intensity. Metallic Au^0 gives rise to a peak at 84.2 eV. After reaction, the doublet of the Au^{3+} shoulders in the Au(4f) spectrum completely disappeared. Obviously, the surface Au oxide species are reduced under reaction conditions. Furthermore, the main Au($4f_{7/2}$) peak shifted to a lower BE of 83.8 eV. The down-shift of the main peaks can originate from the reduction of slightly oxidized Au species (e.g. Au^+ with a BE 0.6 eV higher than that of Au^0 [41;42]) and/or from the significant growth of the ligament size during reaction, from ca. 3.4 nm to ca. 22 nm, as described above. It has been reported that BE shifts of 0.5–0.9 eV relative to the bulk Au^0 value could be obtained as final state effects in small Au clusters [43;44]. With increasing particle size, the Au(4f) peak would shift back to the metallic Au^0 position. In view of the relatively large average Au particle size (3.4 nm) for the fresh sample, however, larger contributions from final state effects are considered to be less likely and thus the higher BE of 84.2 eV of the main peak for the sample before reaction is assigned to contributions from positively charged gold species ($Au^{\delta+}$).

Cu (2p) XP spectra were also recorded before and after reaction to check for the presence of residual Cu and its chemical state(s). The as-prepared NPG(Cu) sample comprises two

components in the BE ranges of 933–934 eV (Cu $2p_{3/2}$) and 953–954 eV (Cu $2p_{1/2}$), respectively, with a spin-orbit coupling energy gap of ca. 20 eV. Both of these peaks are accompanied by distinct satellite peaks at 942 and 962 eV. These features are characteristic of the CuO phase [45-47], which, however, cannot be detected by XRD technique. This can at least partly be explained by the rather low amount of this component, furthermore it indicates that residual Cu is not present as crystalline particles in the sample after leaching (see above). The satellite peaks disappeared after exposure to reaction conditions and the main peak shifted to a lower BE, from 933.5 eV to 931.3 eV, indicating the formation of metallic copper or Cu^+ species [45;47;48]. Due to the presence of the dominant Au($4d_{5/2}$) peak at 335.0 eV, we cannot distinguish between these two species from their Cu LMM Auger peaks at 335.0 eV (Cu^0) or 337.5 eV (Cu^+), respectively. Note that the CuO peaks are still visible in the Cu (2p) spectrum after reaction, although their intensities are much weaker (see Fig. 3b). Quantitative evaluation of the XPS data revealed a Cu concentration of 4.7 at.% in the near surface region accessible to XPS. This value is essentially identical to the bulk concentration of 4.6 at.% determined by EDX. After reaction, the near surface Cu concentration had increased significantly to 8.5 at.%. This increase closely resembles the behavior of Ag in a series of NPG catalysts derived from AuAg alloys, where we also found an enrichment of residual Ag at the surface during the reaction (see also table 1) [21]. This fits well to recent findings that for an as-prepared NPG(Ag) the residual Ag is largely present as small clusters below the surface, whereas after ligament coarsening the Ag is more located at the surface growth [49].

3.2 Surface oxygen species and oxygen storage capacity (OSC) of the NPG(Cu) catalyst

To gain further information on the nature and amount of the oxide species, we performed an O_2-TPD experiment on the catalyst before and after reaction. Figure 4 shows the desorption curves of O_2 (m/z = 32) obtained from the as-prepared sample and that after exposure to

reaction conditions for 2 min and 30 min. The fresh NPG(Cu) catalyst exhibits a pronounced O_2 desorption peak with a maximum at 330ºC, which has previously been assigned to (recombinative) desorption of atomic oxygen species chemisorbed on Au sites or to decomposition of an Au oxide [31]. The distinct O_2 desorption peak completely disappeared after exposure to a flow of reaction gas mixture for 30 min. An additional TPD experiment showed that the low-temperature desorption peak has almost completely disappeared already upon reaction for only 2 min, with the peak area being less than 2% of that for the fresh sample, and the desorption peak shifted to ca. 290°C. Hence, the surface atomic oxygen species present after NPG preparation are rapidly depleted under reaction conditions.

To study the capability of the NPG(Cu) catalyst for O_2 activation (definition see above) and storage of active oxygen, we performed multi-pulse experiments in a TAP reactor, exposing the catalyst first to a sequence of O_2/Ar pulses for oxygen deposition and then to a sequence of CO/Ar pulses for reactive removal of the O_{ad} species (O_{ad} titration). These pulse measurements were performed after removal of the pre-existing surface oxygen with CO pulses, as described already in our previous work [20]. The oxygen uptake increased almost proportionally with the number of O_2 pulses (see Fig. 5), from 0.09×10^{18} O atoms g_{Au}^{-1} after 400 pulses via 0.13×10^{18} O atoms g_{Au}^{-1} after 1000 pulses, 0.24×10^{18} O atoms g_{Au}^{-1} after 2000 pulses to finally 0.41×10^{18} O atoms g_{Au}^{-1} after 4000 pulses (OSCs see Table 2).

Moreover, we also compared the effect of O_2 pulsing with that of continuous exposure to O_2 at atmospheric pressure in a flow of 10% O_2/N_2 (20 Nml min^{-1}, 30°C) after reduction by CO pulses (Fig. 5). Exposure of the NPG(Cu) catalyst to a O_2 gas flow for 30 min gave rise to an oxygen uptake of 1.01×10^{19} O atoms g_{Au}^{-1}, about 42 times higher than that obtained by interaction with 2000 pulses of O_2. Accordingly, the effective probability for active oxygen formation (effective sticking coefficient for dissociative O_2 adsorption), which we define as the fraction of activated oxygen in the total amount of dosed O_2 (O_2 molecules passing

through the catalyst bed), can be estimated to be around 6.3×10^{-6} (total exposure 1.32 mol O_2 g_{Au}^{-1}) (see Table 2). The oxygen uptake can be further enhanced to 1.87×10^{19} O atoms g_{Au}^{-1} and 3.57×10^{19} O atoms g_{Au}^{-1} by prolonging the exposure time to 120 min and 300 min, respectively (see Fig. 5 and Table 2). The influence of the O_2 dosing amount on the OSC of NPG(Cu) closely resembles that for the NPG(Ag) catalyst [20]. Interestingly, the OSC of the NPG(Cu) catalyst is about 5 times lower than that of the Ag-containing NPG sample [20] when measured by O_2 pulsing under the same experimental conditions, but comparable or even higher than that of the NPG(Ag) sample upon exposure to a continuous O_2 gas flow.

Before discussing these differences in the oxygen uptake of NPG(Cu) and NPG(Ag) samples, we will first comment on the much higher oxygen uptake and thus O_2 activation under continuous flow conditions than in the TAP reactor measurements. The much higher OSC values in the former case may first of all be due to the large differences in the effective exposure, while the contact times of the O_2 molecules with the catalyst bed seem to be rather similar in both cases. Under present experimental conditions, they can be estimated to about 0.1 – 0.2 s, both under continuous flow and under pulse conditions (for details see the Supporting Information). As illustrated in Fig. 5, the total exposures differ strongly in both types of measurements, considering that for 2000 O_2/Ar pulses about 10^{19} O_2 molecules are passing through the catalyst bed, while in the continuous flow measurements this amounts to almost 1.6×10^{21} O_2 molecules for 30 min under present conditions, which is by a factor of 160 higher than in the above pulse measurement. The much higher exposure under flow conditions increases the total number of collisions of O_2 with the catalyst, thus leading to a higher amount active oxygen deposition even for the same adsorption probability per collision (see Fig, 5). Considering the different O_2 partial pressures we can estimate the number of collisions of O_2 molecules in the pulse experiments to 2.2×10^{21} collisions per pulse or 4.4×10^{24} per 2000 pulses (Knudsen diffusion, for details see refs. [25;38] and Supporting

Information), while under continuous flow conditions at atmospheric pressure (10% O_2 in N_2, convective flow) the number of collisions for 30 min exposure is about 2.8×10^{26}, i.e., by almost two orders of magnitude higher (see Table 2).

For comparison with NPG(Ag) we calculate the effective initial sticking coefficient S_{eff}, in the initial 400 pulses, which is given by the probability that the O_2 molecules entering the catalyst bed will be adsorbed and form stable adsorbed oxygen species. For the first 400 pulses, the number of adsorbed oxygen atoms per g Au is about 0.09×10^{18}, which corresponds to a total number of 0.18×10^{15} adsorbed O atoms for 2 mg catalyst in the bed. Since exposure to 400 pulses corresponds to 2×10^{18} O_2 molecules, the effective sticking coefficient is 0.45×10^{-4}. Considering that at this point about 1% of the available surface sites are occupied, this should still be close to the initial sticking coefficient, which is supported also by the fact that this value changes only little for the different pulse experiments presented here (see Fig. 5).

For comparison with Surface Science type experiments, where the sticking probability is given per collision, we have to calculate the number of collisions of an O_2 molecule on the way through the catalyst bed. This can be calculated by integrating the collision rate over time (for details see ref. [25;38] and Supporting Information). Given the pulse size of O_2 (0.5×10^{16}) and the temperature (30°C) in this study, the number of collisions of each O_2 molecule with the surface can be estimated to be ca. 0.43×10^6 (see Supporting Information). The effective initial single collision sticking coefficient of O_2 on the NPG(Cu) catalyst $s_{0,sc}$ in the initial 400 pulses can thus be estimated to be

$$S_{0,sc} = 0.45\times10^{-4} / (0.43\times10^{6}) \approx 1.0\times10^{-10}.$$

This value is by several orders of magnitude lower than that on single-crystal Cu(110) surface, which is around 5×10^{-2} [50]. On the other hand, comparing with the NPG(Ag)-2 catalyst, under similar adsorption conditions, it also lower, but only by a factor of 4 ($S_{0,sc} \approx 0.4\times10^{-9}$). As mentioned earlier, although the OSCs of NPG(Cu) is much lower than that of NPG(Ag)

under pulse conditions, the OSC becomes comparable to or even higher on NPG(Cu) relative to NPG(Ag) during continuous O_2 exposure at atmospheric pressure. The plot of the OSC against the O_2 dose (see Fig. 5) shows an almost linear dependence for the NPG(Cu) catalyst in a log-log plot, while for NPG(Ag) the deviations at ambient pressure are much more pronounced. This fact reflects that the effective dissociation probability is almost independent on the pressure on the NPG(Cu) catalyst, whereas this is not the case on NPG(Ag). The reason behind this difference is not yet clear.

We further investigated the stability of the active oxygen species on the NPG(Cu) catalyst by varying the delay time between O_2 and subsequent CO pulses. As shown in Figure 6, there was little variation in the amount of active oxygen species on the surface when increasing the delay time from 4 s to up to 1000 s, indicating that the desorption of adsorbed active oxygen from the NPG(Cu) surface is very slow at 30°C. The high stability of these species points to atomic oxygen as active oxygen species. Similar results were obtained also for the NPG(Ag) catalyst and interpreted in the same way [20].

3.3 Catalytic activity of the NPG(Cu) catalyst

The catalytic activity of the NPG(Cu) catalyst for CO oxidation was first measured by simultaneous pulses of CO/Ar and O_2/Ar in the TAP reactor under UHV conditions, starting with a fresh catalyst. As illustrated in Fig. 7, the CO uptake, which is quantitatively comparable to the amount of CO_2 formation, decreased continuously and eventually was below detection levels (< 1% of the initial activity) after ca. 1500 pulses for 0.6 mg of the NPG(Cu) catalyst. During that time, no measurable O_2 consumption could be detected during the pulse reaction. Apparently, in this experiment CO oxidation proceeds via a non-catalytic process, by reaction of CO molecules with active oxygen species that were already present on the fresh NPG(Cu) catalyst. Similar results have also been obtained previously on the NPG(Ag) catalyst [20] and explained by its poor ability for O_2 activation [20].

In the following experiment, we determined the activity of the NPG(Cu) catalyst in a conventional micro-reactor at atmospheric pressure. Figure 8 shows the CO oxidation activity of the NPG(Cu) catalyst and its development with time on stream in a standard reaction mixture (1% CO, 1% O_2, rest N_2) at 30°C. For the catalyst without pretreatment and reaction in an unfiltered gas stream (no water filter), the activity initially increases steadily for ~2 h, followed by a continuous decay without reaching a steady state. The activity after 1000 min on stream is 3.0×10^{-5} mol_{CO2} s^{-1} g_{Au}^{-1}. A similar reaction behavior was observed in our previous work for the NPG(Ag) catalysts under the same reaction conditions [21]. Wittstock et al. also reported an activation period of approximately 2-3 h at 80°C for a NPG(Ag) disk catalyst, finally reaching either a plateau or, more often, passing through an activity maximum after which the CO_2 production decreased again [7]. In their study, the pristine NPG catalysts were not active for CO oxidation at room temperature. Those authors suggested that the activation phase may be related to the removal of moisture adsorbed in the pores or contaminants stemming from the leaching process, but a definitive reason could not be given in that work.

To check whether such moisture effects exist for the NPG(Cu) catalyst, we performed similar measurements on a catalyst which had been dried before reaction. The catalyst was dried for 15 h in a flow of pure N_2 (20 Nml min^{-1}) at 30ºC, which was passed through a water filter. Subsequently, the catalyst was exposed to a dry reaction gas mixture, which was also passed over a water filter. The temporal evolution of the reaction rate is included in Fig. 8. After an initial activation period of about 5 h the catalyst maintained a very stable reaction rate of ~5.5 $\times10^{-5}$ mol_{CO2} s^{-1} g_{Au}^{-1} over additional 700 min on stream, which is almost double as high as the initial activity (see Fig. 8a). This result is in distinct contrast to our findings for NPG(Ag) catalysts, where the characteristic behavior of the activity, with an initial activation and subsequent deactivation, was maintained also for reaction under dry conditions, after drying

pretreatment and reaction in a dry feed gas, but with lower reaction rates over the entire time of the experiment [21]. To further clarify whether the pronounced difference between 'dry' and 'normal' reaction conditions for the NPG(Cu) catalyst arises from the drying pretreatment of the catalyst or from the use of the water filter in the reaction gas line, we performed a control experiment where the NPG(Cu) catalyst was not dried initially, but where we used dried reaction gases. As shown in Fig. 8, the general trend of the activity is comparable to that obtained for the dry catalyst, only with a slightly higher activity (steady-state reaction rate 6.2 $\times 10^{-5}$ mol_{CO2} s^{-1} g_{Au}^{-1}). Apparently, the residual water content in the NPG(Cu) catalyst, without additional drying treatment, is not sufficient to modify the catalytic activity and stability of the NPG(Cu) catalyst over longer times, it additionally requires the continuous supply with residual water vapor with the reaction gas. The continuous deactivation of the catalyst in the unfiltered feed gas may be attributed to the increasing blocking of active sites by adsorption of water molecules on the catalyst surface. A considerable influence of moisture, beneficial at low concentration below 200 ppm and detrimental at higher concentrations (> 6000 ppm), has also been found for CO oxidation on supported Au/TiO_2 catalysts previously [51-53]. In addition, these results clearly demonstrate that the initial activation phase of the NPG(Cu) catalyst is not affected by drying the catalyst and/or the reaction gases. Based on the results of the structural characterization (see above), we tentatively attribute the initial increase in activity of the NPG(Cu) catalyst to a structural rearrangement of the NPG surface, which is possibly induced by the removal of the pre-existing surface oxide species on the fresh sample, and Cu surface segregation.

The stable activity of the NPG(Cu) catalyst after 1000 min on stream (5.5×10^{-5} mol_{CO} s^{-1} g_{Au}^{-1}) under dry conditions is close to that of the most active NPG(Ag)-2 catalyst (7.5×10^{-5} mol_{CO} s^{-1} g_{Au}^{-1}) reported previously [21] under similar reaction conditions (drying pretreatment, with water filter). If we assume that all surface Au atoms contribute to the reaction, the steady-state

activity of the NPG(Cu) catalyst corresponds to a turnover-frequency (TOF) of 0.4 s^{-1} under present reaction conditions. Considering that the two NPG catalysts have comparable surface areas (9 vs. 10 m^2 g^{-1}) at steady-state, but that the latter contains a much higher surface Ag content under these conditions (30.0 at.%) compared to the Cu surface content of the NPG(Cu) catalyst (8.5 at.%), the activity based on the number of foreign surface atoms (TOF_{Cu}) is about 3 times higher for the NPG(Cu) catalyst (3.7 s^{-1}) than for the NPG(Ag)-2 catalyst based on the number of Ag surface atoms (TOF_{Ag} 1.3 s^{-1}, Table 1). In addition, the NPG(Cu) catalyst and also the NPG(Ag) reference catalyst investigated in this work are also significantly more active in terms of the Au mass-specific reaction rate than the NPG catalysts derived from various Au alloys reported in the literature [6;7;30;54;55] (see Table 3). It is interesting to note that the activity of the NPG(Cu) catalyst with a ligament size of 22 nm under steady-state is comparable to that of a supported Au-Cu/SiO_2 bimetallic catalyst (5.8 $\times 10^{-5}$ mol_{CO} s^{-1} g_{Au}^{-1}, Au/Cu molar ratio 20/1, mean particle diameter 3.6 nm) under similar reaction conditions (1% CO, 1% O_2, He balance, 20 ml min^{-1}) [56].

Finally we want to compare the activity of the NPG(Cu) catalyst during the simultaneous pulse experiments and during the continuous flow experiments. In the simultaneous pulse experiments we could not detect any CO_2 formation, indicating that this was below the detection limit. Assuming that the reaction proceeds i) via formation of O_{ad} and its subsequent reaction with CO_{ad} and ii) in the limits of very low O_{ad} coverages, where each O adatom that is formed is also reacted away, the CO_2 formation per pulse can be estimated from the O_{ad} formation per pulse. We further assume that the O_{ad} formation is not affected by the presence of CO_{ad}. In that case we can calculate the O_{ad} formation from the initial effective sticking coefficient $s_{0,eff}$ for the dissociative adsorption of O_2 during the 400 pulse measurement, which we had determined above to $s_{0,eff}= 0.5\times10^{-4}$. With this value, the uptake of O_{ad} per pulse would be at maximum

$$2\ O_{ad}\ \text{per}\ O_2 \times 5\times10^{15}\ O_2\ \text{per pulse} \times 0.5\times10^{-4} = 5\times10^{11}\ O_{ad}$$

Assuming that all O_{ad} is reacted away, this would also be identical to the formation of 5×10^{11} CO_2 molecules per pulse, which is well below the detection limit of our TAP measurements.

We can compare this estimate with the continuous CO oxidation reaction, assuming again that the reaction is limited by the adsorption of oxygen. The number of O_2 molecules passing through the reactor (1 NmL s^{-1}, 1% O_2) per s can be calculated as

$$0.01 \times (6\times10^{23}\times22400^{-1}) = 2.65\times10^{17}\ O_2 = 5.3\times10^{17}\ \text{O atoms}\ s^{-1}$$

Using the initial effective sticking coefficient of 0.5×10^{-4} derived from the pulse experiments, this would result in a CO_2 formation rate of

$$6\times10^{17}\ \text{O atoms}\ s^{-1} \times 0.5\times10^{-4} = 3\times10^{13}\ CO_2\ \text{molecules}\ s^{-1}$$

On the other hand, in the continuous flow measurements with 1 NmL s^{-1} and 0.527 mg of catalyst, we obtained a CO_2 formation rate (see Fig. 8) of

$$0.4 \times 10^{-4}\ \text{mol}_{CO2}\ g_{Au}^{-1}\ s^{-1} \times (6\times10^{23}) \times 0.000527\ g = 1.26\times10^{16}\ \text{molecules}\ CO_2\ s^{-1}$$

which is by a factor of 400 more than what we had calculated before. This means, that either the oxygen sticking coefficient is vastly higher in the presence of CO than in its absence, or that under these conditions the continuous CO oxidation reaction is dominated by another pathway, which does not involve dissociative adsorption of O_2. In that case a molecular pathway would be most likely as dominant reaction pathway under these conditions, where the reaction takes place between adsorbed CO and adsorbed O_2 species. This would involve a reaction induced or reaction enhanced dissociation of O_2 in the first step. In the next step, the O_{ad} species formed during that process can then easily react with the next CO_{ad}, according to

$$CO_{ad} + O_{2,ad} \rightarrow (CO_{ad}\cdot\cdot O_{2ad})^* \rightarrow O_{ad} + CO_{2,ad}\uparrow \quad (1)$$

$$CO_{ad} + O_{ad} \rightarrow CO_{2,ad}\uparrow \quad (2)$$

This would of course have to be considered also for the simultaneous pulse experiments. But even when increasing the CO_2 formation per pulse by a factor of 400, which is unlikely because of the much lower pressure and thus lower $O_{2,ad}$ and CO_{ad} coverages in the pulses, it would result only in a CO conversion of 5%. This is close to the detection limit, in good agreement with the experimental observation of no detectable CO_2 formation.

In total, this quantitative comparison provides clear evidence that under present reaction conditions CO oxidation on the NPG(Cu) catalyst is dominated by a molecular reaction pathway, while the atomic pathway, via formation of O_{ad} and their subsequent reaction with CO_{ad} to CO_2, is only a minority pathway. The negligible contribution from the atomic pathway results from the very low probability for dissociative oxygen adsorption on the NPG(Cu) catalyst under present reaction conditions, which is considerably lower than on NPG(Ag) catalysts. For the latter catalysts it was found to depend strongly also on the amount of Ag on the surface [21] and on the reaction temperature [24].

3.4 Reaction kinetics of the NPG(Cu) catalyst

The reaction kinetics of the NPG(Cu) catalyst for CO oxidation was further investigated by determining the reaction orders for CO and O_2 for reaction at 30°C under dry reaction conditions. In the first case the CO partial pressure was varied between 0.2 and 2 kPa, at 1 kPa O_2 pressure; in the other measurement, the partial pressure of O_2 was varied from 0.2 to 3 kPa at p_{CO} = 1 kPa. The measurements were performed after running the reaction over 1000 min in the dry feed gas and holding for at least 60 min at each gas composition until steady-state conditions were reached. The results are presented in Fig. 9 and Table 3. The reaction orders determined from the slopes of the plots are 0.68 and 0.38 for CO and O_2, respectively. Similar kinetic experiments performed on the NPG(Ag)-2 catalyst resulted in reaction orders of 0.62 for CO and 0.51 for O_2, respectively (Table 3). It should be noted that the activity measurements were performed under differential reaction conditions, with conversions below

15% for CO and O_2, and that based on an estimate of the Thiele modulus (<3) the influence of mass transport phenomena on the measured reaction kinetics was negligible.

The positive reaction orders for both reactants and on both catalysts indicate that the reaction is not limited by site blocking by one of the two reactants, neither for the NPG(Cu) nor for the NPG(Ag)-2 catalyst. Instead, the supply of reactants must be limiting. The comparable reaction orders for CO for the two catalysts may be considered as evidence for a similar reaction mechanism on both catalysts, although such conclusions, on the basis of similar kinetic details, have to be taken with caution. The discrepancy in the reaction orders for O_2 would be consistent with a mechanism where the second metal, i.e., Cu or Ag surface atoms, plays an essential role for the adsorption and activation of O_2 on the NPG catalysts.

From kinetic measurements on various NPG(Ag) disk samples with different Ag contents, Wittstock et al. found that for all samples the reaction orders for O_2 are around 0, whereas the values for CO varied between 0 and 1 [7]. Xu et al. [6] reported reaction orders of 0.78 and 0.25 for CO and O_2, respectively, on a powder NPG catalyst at reaction temperatures of -10°C and 0°C (20 mg catalyst, Ag bulk content ~3 at.%, 1% CO / 10% O_2 / 89% N_2, flow rate 66.7 ml min^{-1}). One should consider, however, that these reaction rates were estimated from CO conversions of up to 70%.

We also determined the apparent activation energy for the CO oxidation reaction in the standard reaction mixture (1 kPa CO, 1 kPa O_2, N_2 as balance) on the NPG(Cu) catalyst from the temperature dependence of the rates between 30 and 150ºC under dry reaction conditions (see above). After reaction at 30ºC in the dry feed gas for 1000 min to reach steady-state, the temperature was raised stepwise by 15ºC every two hours up to 150ºC. Finally, the reactor was cooled down to 30ºC to check if there was any activity loss induced by reaction at higher temperatures. As shown in Fig. 10, there are three temperature regimes with different evolution of the activity with time. At 30° and 45°C, the reaction rate remained largely

constant with time, at higher temperatures up to 90°C it decayed with time from an initially higher value, and when the temperature was raised further, it increased initially. This effect was most pronounced at 105° and 120°C, while at higher temperatures the changes were rather small. Finally, upon adjusting the temperature back to 30ºC, the catalyst was found to be as active as before the heat-up procedure. The latter fact demonstrates that within the temperature range covered in these measurements the Cu-containing NPG catalyst is not affected by irreversible structural modifications.

Note that in the medium temperature range, between 60 and 90°C, the activity decreases not only with time on stream, but also with temperature. As mentioned above, this unexpected temperature-induced catalytic behavior cannot be attributed to structural coarsening or sintering, which should lead to irreversible activity losses. Moisture effects, as suggested by Daté et al. for supported Au/SiO_2 catalysts [52], can also be excluded, since the measurements were performed under dry conditions. A similar decay in activity with increasing temperature has been reported earlier for CO oxidation on a series of Au-Ag alloy catalysts supported on mesoporous aluminosilicate materials (decay from 80 to 160°C, 1% CO, 4% O_2, balanced with He, 66.7 mL min^{-1}) [57] as well as on the Au-Cu bimetallic catalysts supported on silica gel (decay from 30 to 100°C, 1% CO, 1% O_2, balanced with He, 20 mL min^{-1}) [56]. In contrast, this phenomenon was not observed on their pure metallic counterparts, i.e., on supported Au or supported Ag catalysts [57]. In addition, the critical temperature where the activity starts to decrease was found to depend on the Au/Ag composition [57]. When the reaction temperature was further enhanced, the activity would increase again in light-off curves. It was proposed that this unusual temperature dependence of the activity is associated with a reversible change in the reaction pathways, from a low-temperature reaction pathway a high-temperature reaction pathway and vice versa [56]. A complex temperature dependence of the CO oxidation activity with a decrease in activity between -50 and +20°C was reported

recently also for CO oxidation on a $Au/Mg(OH)_2$ catalyst [58-62]. The authors of two recent studies provided clear evidence that this behavior results from a change in the rate-determining step or reaction pathway [61;62]. Such kind of change in the reaction mechanism or at least in the rate limiting step is also likely to occur in the NPG catalyst system. For example, one could speculate that in the low-temperature range the reaction proceeds mainly by reaction between molecularly adsorbed species, between $O_{2,ad}$ and CO_{ad} (see previous section) and that this process is activated, which would lead to an increasing reaction rate with increasing temperature In the medium temperature range, desorption of the adsorbed species (CO_{ad} and $O_{2,ad}$) could start to dominate the reaction behavior via a decreasing surface coverage, which results in a decreasing rate with increasing temperature. In the higher temperature range, finally, one may assume that the reaction proceeds mainly via O_{ad}, whose formation and subsequent reaction with CO_{ad} are activated. This would result again in an increase of the reaction rate with temperature. Here we would like to note that this temperature dependence is not specific for NPG(Cu), similar effects were also observed for NPG(Ag) catalysts in our experiments (see Supporting Information).

Finally, in order to estimate the apparent activation energy, the activity at 30 ºC together with the initial activities at 45ºC and 60ºC were plotted in an Arrhenius plot (inset in Fig. 10). Another plot taking the initial activities from 105 to 150ºC is also included for comparison. They result in apparent activation energies (E_a) of 10.8±1.3 kJ mol^{-1} and 20.2±0.6 kJ mol^{-1} for the low-temperature and higher-temperature region, respectively. The former value is comparable to that reported for CO oxidation on NPG(Cu) catalysts previously [54;55], but smaller than the values determined for the NPG(Ag) catalysts. An apparent E_a of 5-6 kJ mol^{-1} was reported for CO oxidation (60 - 150°C, 4% CO, 2% O_2, balanced with He, 50 mL min^{-1}) on NPG(Cu) catalysts, which were prepared by leaching of $AuCu_3$ alloys, whose surface Cu content was not specified [54] (see Table 3). In a more recent work, an apparent E_a of ca. 12.5

kJ mol^{-1} was obtained from CO oxidation rates measured on a NPG(Cu) catalyst (-40 to 0°C, 1% CO, 10% O_2, balanced with N_2, 66.7 mL min^{-1}), which was derived from a AuCu alloy via electrochemical de-alloying [55]. Note that in both cases the reaction rates were determined by using high conversion data (>20%), and possible effects of mass transport limitations were not excluded. We also performed similar experiments to determine the apparent activation energy on the NPG(Ag)-2 catalyst, but this led to a continuous decay in the activity with both time and temperature above 30ºC (see Supporting Information).

3.5 Nature of the active sites on the NPG(Cu) catalyst for CO oxidation

The nature of the sites for the adsorption and activation of O_2 molecules is of central importance for the mechanistic understanding of the CO oxidation reaction on the NPG catalysts. The controversy on this topic is largely related to the role of residual impurities of the second metal (Ag, Cu, etc., depending on the starting material) in the reaction. Most recently, using spherical-aberration-corrected transmission electron microscopy (TEM) and environmental TEM, Fujita et al. [22] observed a high density of atomic steps and kinks on the curved surfaces of NPG (1.2 at.% Ag residue, ligament size 30 nm), which was comparable to that in 3–5 nm nanoparticles. Comparing two NPG samples with different Ag contents under a CO/air reaction atmosphere at 30 Pa at room temperature, they found that the {111} faceting dynamics is significantly slower on the sample with high Ag content, which also exhibited the superior catalytic activity in the CO oxidation reaction. Based on these *in situ* TEM observations, they proposed that the surface defects are active sites for the catalytic oxidation of CO and that residual Ag stabilizes the atomic steps by suppressing the {111} faceting kinetics. Although this study provided clear evidence that the high activity of the NPG catalyst is related to the presence of step and defect sites, it could not distinguish the respective role of Au and residual Ag in the catalytic reaction.

Aiming at clarifying the intrinsic catalytic activity of gold, Déronzier et al. [30] synthesized a

NPG material (9 m^2 g^{-1}, 20 nm crystallite size by XRD) with an ultra-low residual Zr bulk content of 0.03 at.% by leaching of zirconia from an oxidized $Au_{0.5}Zr_{0.5}$ intermetallic alloy. They found that this NPG catalyst shows a CO conversion of only 2% at 140ºC (200 mg catalyst, 2% CO + 2% O_2 + 96% He, 50 ml min^{-1}), which corresponds to a TOF of at least about 3 orders of magnitude below that reported for other Ag- or Cu-containing NPG catalysts [5;6;54]. Since the XPS spectra showed no detectable Zr residues, the catalytic activity was attributed to gold alone. These authors suggested that the low activity is probably related to a low concentration of low-coordination active sites present at the surface [30], which seems to be in good agreement with the conclusions by Fujita et al. [22].

From experimental and theoretical studies [63-66] it is known that the dissociative adsorption of O_2 on Au surfaces could be possible if significant fractions of low-coordination gold atoms such as step or kink sites exist or at elevated temperatures. Compared with the almost pure NPG(Zr) sample, the much higher catalytic activities of the Ag- or Cu-containing NPG catalysts with similar structural properties (similar ligament sizes, 20 - 30 nm) strongly suggest that the Ag or Cu residues play an important role in the dissociative adsorption of O_2. In fact, we have shown previously [21] that the amount of active oxygen adsorbed on NPG(Ag) samples is about linearly related to the amount of surface Ag, providing strong evidence that the activation of molecular oxygen, which itself is only weakly adsorbed, takes place at sites connected to surface Ag (either directly on the Ag surface atom or at ensembles including surface Ag atoms). The direct influence of changes in surface Ag concentration and dynamic restructuring at the nanoscale on oxidation activity has also been demonstrated by *in situ* TEM and XPS characterization recently [29]. Similar to the NPG(Ag) catalyst, the results in the present work clearly indicate that despite the significantly lower surface Cu content, the NPG(Cu) catalyst is also able to activate O_2 for dissociative adsorption at 30°C (Fig. 5). The exact form of generated active oxygen species, however, may depend on the experimental

conditions.

Duan et al. recently prepared NPG catalysts from AuAl and AuCu alloys by electrochemical dealloying [55]. They found about similar conversions for CO oxidation on NPG with Al_2O_3 residues (surface Al 0.3 at.%) and on NPG with CuO residues (surface Cu 2.4 at.%), as determined by XPS, under identical reaction conditions. In additional experiments these authors also explored the effect of residual metallic Cu or Al on the surface, using NPG catalysts with different Cu bulk (4.9 and 6.6 at.%) or Al bulk (3.27 and 6.21 at.%) contents, as determined by EDX. Since they did not observe any significant effect of the Cu or Al bulk concentration on the activity of the NPG catalysts, they suggested that the residual metals or metal oxides have no significant effect on the intrinsic activity of the NPG catalyst. It should be noted, however, that in the latter case the surface contents of Cu or Al residues, particularly those after reaction, were not examined. Furthermore, the CO oxidation activity was mostly determined at sub-ambient temperature between -40 and +30 °C, where the active sites and reaction mechanism for CO oxidation may be distinctly different from that above room temperature [67]. Nevertheless, these results show that cautions should be taken when comparing the catalytic properties of NPG catalysts under different reaction conditions.

Finally, Liu et al. investigated a series of Au-Cu bimetallic catalysts supported on mesoporous silica material (SBA-15) and found that the bimetallic catalysts showed a superior performance in the CO oxidation reaction compared to monometallic gold catalysts on the same support material [56]. Furthermore, *in situ* X-ray absorption spectra revealed that for all catalysts only metallic Au species were present under CO oxidation conditions, whereas Cu^0 in the bimetallic Au-Cu catalyst was easily oxidized to Cu^+ and Cu^{2+} during CO oxidation, forming small islands of CuO_x on the gold surface [68]. This strongly suggests that oxygen can be activated at the Cu sites. This result agrees closely with findings in the present work, where XPS spectra collected on the NPG(Cu) catalyst after reaction (Fig. 3) also showed that

part of the surface copper species were still in an oxidized state, while the surface Au species were completely reduced. Here it should be noted that the XPS spectra contain information of the topmost few layers, which means that we cannot rule out that most or all of the Cu surface species are in an oxidized state. A close analogy between the NPG(Cu) catalyst and AuCu bimetallic catalysts is observed also for the temperature-dependent CO oxidation activity, which for both catalysts showed the same complex characteristics (Fig. 10). The distinct agreement of the reaction behavior of both catalysts strongly suggests that Au and Cu surface atoms both contribute in a synergetic way to the CO oxidation activity of the NPG(Cu) catalyst, with CO mainly adsorbed on Au^0 sites and active oxygen provided by the neighboring Cu surface atoms or Cu-containing ensembles, similar to the reaction behavior proposed previously for NPG(Ag) catalysts [21].

4. Conclusions

Aiming at a better understanding of the role of second metal trace impurities in the CO oxidation reaction on nanoporous gold (NPG) catalysts we have prepared a NPG catalyst by electrochemical dealloying of a AuCu alloy and investigated its oxygen adsorption and CO oxidation behavior. Structure and surface composition of the fresh catalyst and after reaction were characterized by SEM, XRD and XPS. Comparing also with results of similar measurements on a NPG(Ag) catalyst, under similar adsorption / reaction conditions, we arrive at the following conclusions:

1. Based on a combination of SEM, XRD, XPS and TPD data the pre-existing surface oxygen species on the as-prepared NPG surface is rapidly reduced during the CO oxidation reaction, within few minutes. This goes along with a slower, but severe structural coarsening of the NPG(Cu) catalyst and an increase in surface Cu during reaction, similar to observations for the NPG(Ag) catalyst. For both catalysts, this is accompanied by a slow activation of the catalyst during the first few hours, most likely

induced by the structural modification and the increase in surface Cu during reaction.

2. Both the effective initial sticking coefficient and the single collision (Surface Science type) initial sticking coefficient for dissociative oxygen adsorption are significantly smaller on the NPG(Cu) catalyst than on the NPG(Ag) catalyst, based on multipulse TAP measurements. Based on its stability, this species must be atomic oxygen. A much higher oxygen uptake during exposure to O_2 at atmospheric pressure compared to multipulse deposition is mainly attributed to the much higher integrated O_2 exposure in the latter case rather than to pressure effect.
3. Comparing the experimentally observed CO_2 formation rate under continuous flow conditions, at atmospheric pressure, with a rate calculated based on the assumption that i) O_{ad} formation is the rate limiting step and subsequent reaction with CO_{ad} is fast and that ii) O_{ad} formation is not enhanced by the presence of CO_{ad}, but is at most equal to the rate determined by the initial O_2 sticking coefficient, reveals that the experimentally measured rate is at least by a factor of 400 higher than the calculated rate. Based on this result we propose that for the NPG(Cu) catalyst reaction via O_{ad} formation and subsequent reaction with CO_{ad} is only a minority pathway under present reaction conditions (30°C), while most of the reaction proceeds via a molecular mechanism, including either a CO_{ad} assisted dissociation of molecularly adsorbed $O_{2,ad}$ or reaction between CO_{ad} and $O_{2,ad}$ to form CO_2 and O_{ad}, where the latter is rapidly reacted away subsequently. This interpretation is supported also by the complex reversible temperature dependence of the reaction rate, which we found to be characteristic for both NPG(Cu) and NPG(Ag) in our studies.
4. Finally we have shown that the catalytic activity and stability of the NPG(Cu) catalyst can be significantly affected by moisture in the feed gas. Moisture effects were observed also for NPG(Ag), but the trends were different. Under dry reaction conditions, the reaction orders for CO and O_2 were determined to be 0.68 and 0.38, respectively, with apparent

activation energies of ca. 10.8±1.3 kJ mol^{-1} and 20.2±0.6 kJ mol^{-1} in the low and higher temperature regime, respectively, which is also somewhat different from NPG(Ag) catalyst.

Based on these results, the residual surface Cu in the NPG(Cu) catalyst is proposed to play an important role in O_2 activation, both for stable oxygen adsorption and for CO oxidation, similar to that of Ag surface impurities in the NPG(Ag) catalysts.

Acknowledgements

This work was supported by the Baden-Württemberg Stiftung within the Network 'Functional Nanostructures'. L.-C. Wang is grateful for a fellowship from the Alexander-von Humboldt-Foundation. We gratefully acknowledge T. Diemant for XPS measurements, U. Hörmann for SEM measurements and S. Blessing for XRD analysis (all Ulm University).

References

1. Haruta M, Kobayashi T, Sano H, and Yamada N (1987) Chem Lett 16: 405 - 408
2. Haruta M (1997) Catal Surv Jap 1: 61 - 73
3. Haruta M (2002) Cattech 6: 102 - 115
4. Bond,GC, Louis,C, and Thompson,DT (2007) Catalysis by Gold, Imperial Press, London
5. Zielasek V, Jürgens B, Schulz C, Biener J, Biener MM, Hamza AV, and Bäumer M (2006) Angew Chem Int Ed 45: 8241 - 8244
6. Xu C, Xu X, Su J, and Ding Y (2007) J Catal 252: 243 - 248
7. Wittstock A, Neumann B, Schaefer A, Dumbuya K, Kübel C, Biener MM, Zielasek V, Steinrück HP, Gottfried JM, Biener J, Hamza A, and Bäumer M (2009) J Phys Chem C 113: 5593 - 5600
8. Wittstock A, Zielasek V, Biener J, Friend CM, and Bäumer M (2010) Science 327: 319 - 322
9. Krajci M, Kameoka S, and Tsai AP (2017) J Chem Phys 147: 044713 - 044713-14
10. Li D, Zhu Y, Wang H, and Ding Y (2013) Sci Rep 3: 3015 - 3015-7
11. Deronzier T, Morfin F, Lomello M, and Rousset J-L (2014) J Catal 311: 221 - 229
12. Wittstock A, Wichmann A, Biener J, and Baumer M (2011) Faraday Discuss 152: 87 - 98
13. Kosuda KM, Wittstock A, Friend CM, and Bäumer M (2012) Angew Chem Int Ed 51: 1698 - 1701
14. Wang LC, Stowers KJ, Zugic B, Personick ML, Biener MM, Biener J, Friend CM, and Madix RJ (2015) J Catal 329: 78 - 86
15. Pedireddy S, Lee HK, Tjiu WW, Phang IY, Tan HR, Chua SQ, Troadec C, and Ling XY (2014) Nat Commun 5: 4947 - 4947-9
16. Xu H, Shen K, Liu S, Zhang L, Wang X, Qin J, and Wang W (2016) J Phys Chem C 120: 25296 - 25305

17. Yan M, Jin T, Ishikawa Y, Minato T, Fujita T, Chen LY, Bao M, Asao N, Chen MW, and Yamamoto Y (2012) J Am Chem Soc 134: 17536 - 17542

18. Takale BS, Feng X, Lu Y, Bao M, Jin T, Minato T, and Yamamoto Y (2016) J Am Chem Soc 138: 10356 - 10364

19. Xu C, Su J, Xu X, Liu P, Zhao H, Tian F, and Ding Y (2007) J Am Chem Soc 129: 42 - 43

20. Wang LC, Jin H-J, Widmann D, Weissmüller J, and Behm RJ (2011) J Catal 278: 219 - 227

21. Wang LC, Zhong Y, Widmann D, Weissmüller J, and Behm RJ (2012) ChemCatChem 4: 251 - 259

22. Fujita T, Guan P, McKenna K, Lang X, Hirata A, Zhang L, Tokunaga T, Arai S, Yamamoto Y, Tanaka N, Ishikawa Y, Asao N, Yamamoto Y, Erlebacher J, and Chen M (2012) Nature Mater 11: 775 - 780

23. Liu P, Guan P, Hirata A, Zhang L, Chen L, Wen Y, Ding Y, Fujita T, Erlebacher J, and Chen M (2016) Adv Mater 28: 1753 - 1759

24. Wang LC, Friend CM, Fushimi R, and Madix RJ (2016) Faraday Discuss 188: 57 - 67

25. Wang LC, Personick ML, Karakalos S, Fushimi R, Friend CM, and Madix RJ (2016) J Catal 344: 778 - 783

26. Montemore MM, Madix RJ, and Kaxiras E (2016) J Phys Chem C 120: 16636 - 16640

27. Kameoka S, Tanabe T, Miyamoto K, and Tsai AP (2016) J Chem Phys 144: 034703 - 034703-8

28. Krajci M, Kameoka S, and Tsai AP (2016) J Chem Phys 145: 084703 - 084703-6

29. Zugic B, Wang LC, Heine C, Zakharov DN, Lechner BAJ, Stach EA, Biener J, Salmeron M, Madix RJ, and Friend CM (2017) Nat Mater 16: 558 - 564

30. Deronzier T, Morfin F, Massin L, Lomello L, and Rousset J-L (2011) Chem Mater 23: 5287 - 5289

31. Wang L-C, Zhong Y, Yin H, Widmann D, Weissmüller J, and Behm RJ (2013) Beilstein J Nanotechnol 4: 111 – 128

32. Zhong YX, Yan JW, Li MG, Zhang X, He DW, and Mao BW (2014) J Am Chem Soc 136: 14682 - 14685

33. Trasatti S and Petrii OA (1991) Pure Appl Chem 63: 711 - 734

34. Jin HJ, Parida S, Kramer D, and Weissmüller J (2008) Surf Sci 602: 3588 - 3594

35. Kahlich MJ, Gasteiger HA, and Behm RJ (1997) Journal of Catalysis 171: 93 - 105

36. Schubert MM, Hackenberg S, van Veen AC, Muhler M, Plzak V, and Behm RJ (2001) J Catal 197: 113

37. Leppelt R, Hansgen D, Widmann D, Häring T, Bräth G, and Behm RJ (2007) Rev Sci Instrum 78: 104103-1 - 104103-9

38. Gleaves JT, Yablonskii GS, Phanawadee P, and Schuurman Y (1997) Appl Catal A 160: 55 - 88

39. Parida S, Kramer D, Volkert CA, Rösner H, Erlebacher J, and Weissmüller J (2006) Phys Rev Lett 97: 035504 - 035504-1

40. Jin H-J, Wang X-L, Parida S, Wang K, Seo M, and Weissmüller J (2009) Nano Lett 10: 187 - 194

41. Fu Q, Saltsburg H, and Flytzani-Stephanopoulos M (2003) Science 301: 935 - 938

42. Deng W, Carpenter C, Yi N, and Flytzani-Stephanopoulos M (2007) Top Catal 44: 199 - 208

43. Haruta M, Tsubota S, Kobayashi T, Kageyama H, Genet MJ, and Delmon B (1993) J Catal 144: 175 - 192

44. Boyen H-G, Ethirajan A, Kästle G, Weigl F, Ziemann P, Schmid G, Garnier MG, Büttner M, and Oelhafen P (2005) Phys Rev Lett 94: 016804-1 - 016804-1

45. L.Alejo, R.Lago, M.A.Pena, and J.L.G.Fierro (1997) Appl Catal A 162: 281 - 297

46. Agrell J, Birgersson H, Boutonnet M, Melian-Cabrera I, Navarro RM, and Fierro JLG (2003) J Catal 219: 389 - 403

47. Matter PH, Braden DJ, and Ozkan US (2004) J Catal 223: 340 - 351

48. Dai W-L, Sun Q, Deng J-F, Wu D, and Sun Y-H (2001) Appl Surf Sci 177: 172 – 179

49. Krekeler T, Straßer AV, Graf M, Wang K, Hartig C, Ritter M, and Weissmüller J (2017) Mater Res Lett 5: 314 - 321

50. Wachs IE and Madix RJ (1978) J Catal 53: 208 - 227

51. Daté M and Haruta M (2001) J Catal 201: 221 - 224

52. Daté M, Okumura M, Tsubota S, and Haruta M (2004) Angew Chem 116: 2181 - 2184

53. Saavedra J, Doan HA, Pursell CJ, Grabow LC, and Chandler BD (2014) Science 345: 1599 - 1602

54. Kameoka S and Pang Tsai A (2008) Catal Lett 121: 337 - 341

55. Duan H and Xu C (2015) J Catal 332: 31 - 37

56. Liu X, Wang A, Zhang T, Su DS, and Mou C-Y (2011) Catal Today 160: 103 - 108

57. Wang A-Q, Liu J-H, Lin SD, Lin T-S, and Mou C-Y (2005) J Catal 233: 186 - 197

58. Cunningham DAH, Vogel W, and Haruta M (1999) Catal Lett 63: 43 - 47

59. Margitfalvi JL, Fasi A, Hegedus M, Lonyi F, Gobolos S, and Bogdanchikova N (2002) Catal Today 72: 157 - 169

60. Jia CJ, Liu Y, Bongard H, and Schüth F (2010) J Am Chem Soc 132: 1520 - 1522

61. Wang Y, Lehnert F, Widmann D, Gu D, Schüth F, and Behm RJ (2017) Angew Chem Int Ed 56: 9597 - 9602

62. Wang, Y., Widmann, D., Wittmann, M., Lehnert, F., Gu, D., Schüth, F., and Behm, R. J. (2017) Catal Sci Technol 7: 4145 - 4161.

63. Liu Z-P, Hu P, and Alavi A (2002) J Am Chem Soc 124: 14770 - 14779

64. Lopez N, Janssens TVW, Clausen BS, Xu Y, Mavrikakis M, Bligaard T, and Nørskov JK (2004) J Catal 223: 232 - 235

65. Janssens TVW, Carlsson A, Puig-Molina A, and Clausen BS (2006) J Catal 240: 108 - 113

66. Roldan A, Gonzalez S, Ricart JM, and Illas F (2009) ChemPhysChem 10: 348 - 351

67. Green IX, Tang W, Neurock M, and Yates JT (2011) Science 333: 736 - 739

68. Liu X, Wang A, Li L, Zhang T, Mou C-Y, and Lee JF (2011) J Catal 278: 288 – 296

Table 1: Comparison of the physical properties, oxygen storage capacity (OSC) and catalytic activity in CO oxidation at 30°C between NPG(Cu) and NPG(Ag)-2 [21] catalysts.

Catalyst	NPG(Cu)-fresh	NPG(Cu)-used	NPG(Ag)-2-fresh	NPG(Ag)-2-used
Surface area / $m^2\ g^{-1}$ [c]	49	n.d. [a]	63	n.d.
Average crystallite size D / nm [b]	3.4	22	6.4	20.6
Surface area estimated from D / $m^2\ g^{-1}$ [d]	60	9	31	10
Bulk Cu or Ag / at.% [e]	4.6	n.d.	13.2	n.d.
Surface Cu or Ag / at.% [f]	4.7	8.5	9.5	30.0
Surface Au atoms / $10^{20}\ g_{cat}^{-1}$	3.9	0.94	6.6	0.80
Surface Cu or Ag atoms / $10^{20}\ g_{cat}^{-1}$	0.19	0.09	0.69	0.34
OSC / 10^{19} O atoms g_{Au}^{-1} (exposure 30 min)	1.0	0.26	1.4	1.2
r_{Au} / $10^{-5}\ mol_{CO}\ s^{-1} g_{Au}^{-1}$	2.9	3.0	12.4	9.2
r_{Au}-dry / 10^{-5} mol $s^{-1}\ g_{Au}^{-1}$ [g]	3.0	5.5	9.9	7.5
TOF(Au)-dry / s^{-1}	0.05	0.4	0.09	0.6
TOF(Cu or Ag)-dry / s^{-1}	1.0	3.7	0.9	1.3

[a] not determined.

[b] estimated from Au(111) diffraction peaks by using the Scherrer equation.

[c] surface areas of the fresh samples measured by capacitance ratio method.

[d] estimated by assuming idealized, cylindrical ligaments with diameter D.

[e] measured by SEM-EDX.

[f] determined by XPS.

[g] reaction rate measured after drying pre-treatment with water filter.

Table 2: Stable oxygen uptake in pulse experiments (5×10^{15} O_2 molecules per pulse, 2 mg Au) and continuous O_2 exposure at atmospheric pressure (10% O_2 in N_2, 20 NmL min^{-1}, 2 mg Au) and the initial sticking coefficients derived from the 400 multi-pulse sequence (all experiments at 30°C).

Experiment	Total O_2 exposure / 10^{18} O_2 molecules	Total O_2 exposure / 10^{21} O_2 molecules g_{Au}^{-1}	Stable oxygen uptake / 10^{18} O_{ad} atoms g_{Au}^{-1}	Integrated effective sticking coefficient
400 pulses O_2/Ar	2	1	0.09	0.45×10^{-4}
1000 pulses O_2/Ar	5	2.5	0.13	0.26×10^{-4}
2000 pulses O_2/Ar	10	5	0.24	0.24×10^{-4}
4000 pulses O_2/Ar	20	10	0.41	0.21×10^{-4}
30 min continuous exposure	1600	800	10.1	6.3×10^{-6}
120 min continuous exposure	6400	3200	18.7	2.9×10^{-6}
300 min continuous exposure	16000	8000	35.7	2.2×10^{-6}
Initial effective sticking coefficient (400 pulse expt.)				0.45×10^{-4}
Initial single collision sticking coefficient (400 pulse expt.)				1.0×10^{-10}

Table 3: Kinetic parameters for the CO oxidation reaction at 30°C over various Au catalysts and relevant reaction conditions.

Catalyst	T / ºC	r / 10^{-5} mol s^{-1} g_{Au}^{-1}	α_{CO}	α_{O2}	E_a / kJ mol^{-1}	Ref.
NPG(Cu) (under dry conditions)	30	5.5	0.68	0.38	10.8	This work
Porous Au (ordered $AuCu_3$)	60	2.0	n.r. [a]	n.r.	5	[54]
Porous Au (disordered $AuCu_3$)	60	1.6	n.r.	n.r.	6	[54]
NPG(Cu)	30	4.1	n.r.	n.r.	12.5 [c]	[55]
NPG(Al)	30	4.0	n.r.	n.r.	13.8 [c]	[55]
$Au_{20}Cu_1/SiO_2$	30	5.8	n.r.	n.r.	n.r.	[56]
NPG(Ag)-2 (under dry conditions)	30	7.5	0.62	0.51	n.d. [b]	[21]
NPG(Ag)	30	1.3	0.78	0.25	28.8	[6]
NPG(Ag)	30	1.9	0.5 ~ 1	0.50	31	[7]

[a] not reported.

[b] not determined.

[c] Calculated from the activity results at different temperatures.

Figure Captions

Figure 1: SEM images of the NPG(Cu) catalyst before and after 1000 min on stream.

Figure 2: XRD patterns of the NPG(Cu) catalyst before and after 1000 min on stream.

Figure 3: Au(4f) (a) and Cu(2p) (b) XP spectra of the NPG(Cu) catalyst before and after 1000 min on stream.

Figure 4: TPD spectra of oxygen species (m/z = 32) before reaction and after reaction for 2 min and 30 min.

Figure 5: Effect of the O_2 exposure on the amount of O_{ad} formed on the NPG(Cu) and NPG(Ag) catalyst, as detected by the CO_2 produced upon subsequent CO pulsing. Oxygen was deposited either by O_2/Ar pulses or by exposure to 10% O_2/N_2 (20 Nml min^{-1}, atmospheric pressure) for 30 min, 120 min and 300 min.

Figure 6: Accumulated amount of CO_2 produced by 50 pulses of CO/Ar following 1000 pulses of O_2/Ar with different time delays.

Figure 7: Accumulated uptake of CO and O_2 and CO_2 formation during simultaneous pulsing of CO/Ar and O_2/Ar pulses on the fresh NPG(Cu) catalyst in the TAP reactor (0.6 mg NPG(Cu) catalyst diluted with SiO_2 (1:10), reaction temperature 30°C, 1×10^{16} molecules per pulse, with CO:Ar and O_2:Ar = 1:1).

Figure 8: (a) Catalytic activities and (b) deactivation of the NPG(Cu) catalyst measured in a micro-reactor under differential reaction conditions with or without drying. (reaction temperature 30°C, 60 Nml min^{-1}:1% CO/1% O_2/ rest N_2, atmospheric pressure).

Figure 9: Determination of the reaction order of CO (0.2–3.5 kPa CO) and O_2 (0.2–1.7 kPa O_2) on the NPG(Cu) catalyst at 30ºC (reaction temperature 30°C, 60 Nml min^{-1}:1%

CO/1% O_2/ rest N_2, atmospheric pressure). Changes in the gas composition were compensated by N_2.

Figure 10: The temporal evolution of CO oxidation reaction rates (mol_{CO2} s^{-1} g_{cat} $^{-1}$) at different temperatures over the NPG(Cu) catalyst after 1000 min reaction to reach steady-state conditions and the Arrhenius plot of the temperature-dependent activities at 30ºC, 45ºC and 60ºC.

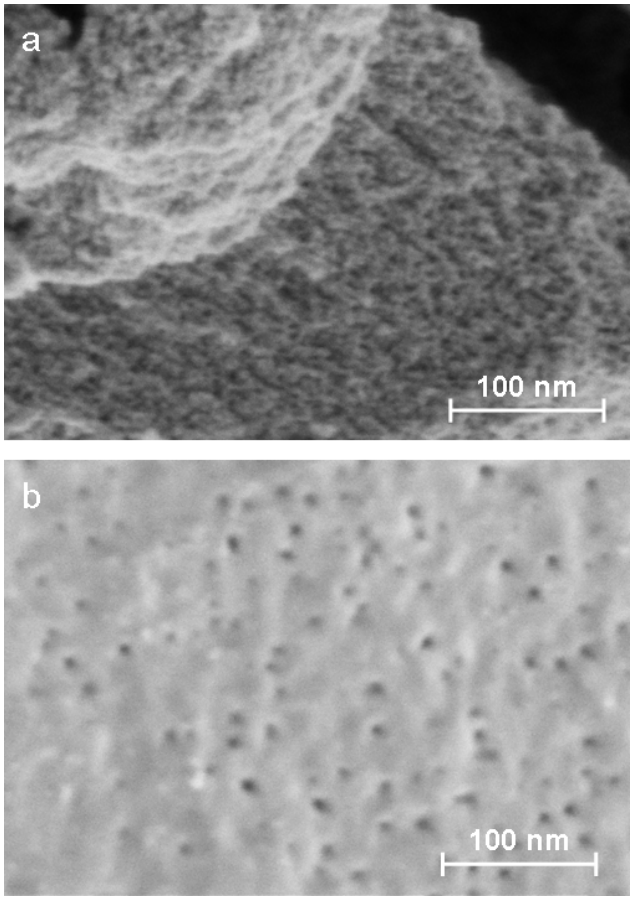

Fig. 1 L.-C. Wang et al.

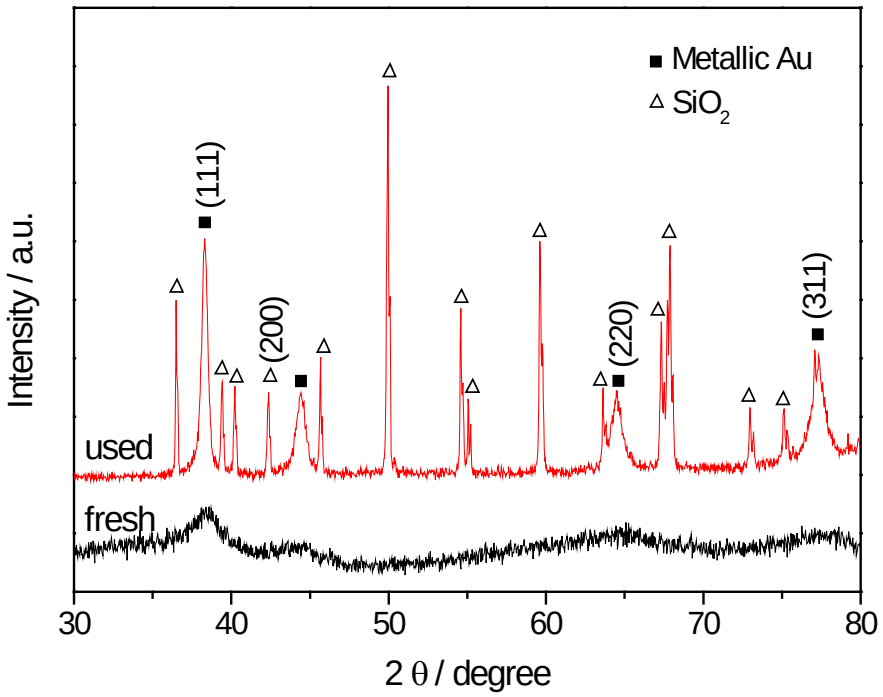

Fig. 2 L.-C. Wang et al.

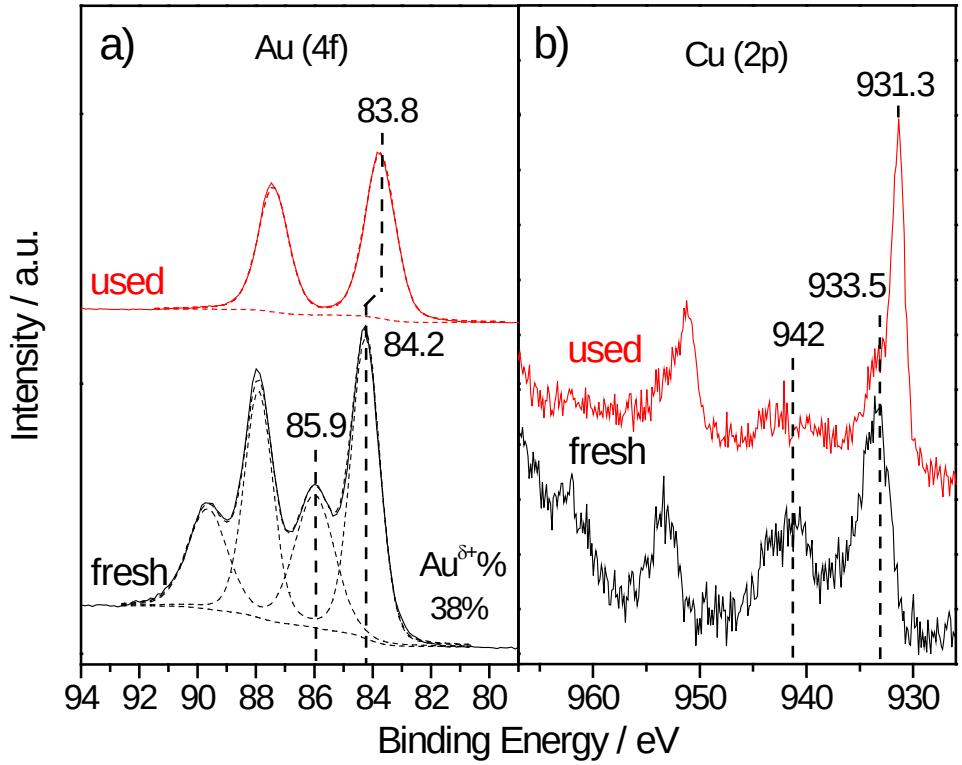

Fig. 3 L.-C. Wang et al.

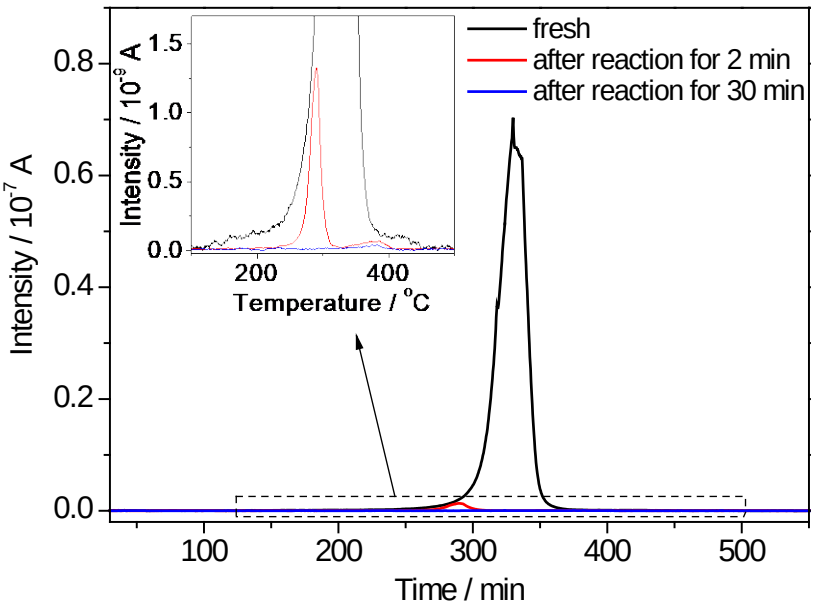

Fig. 4 L.-C. Wang et al.

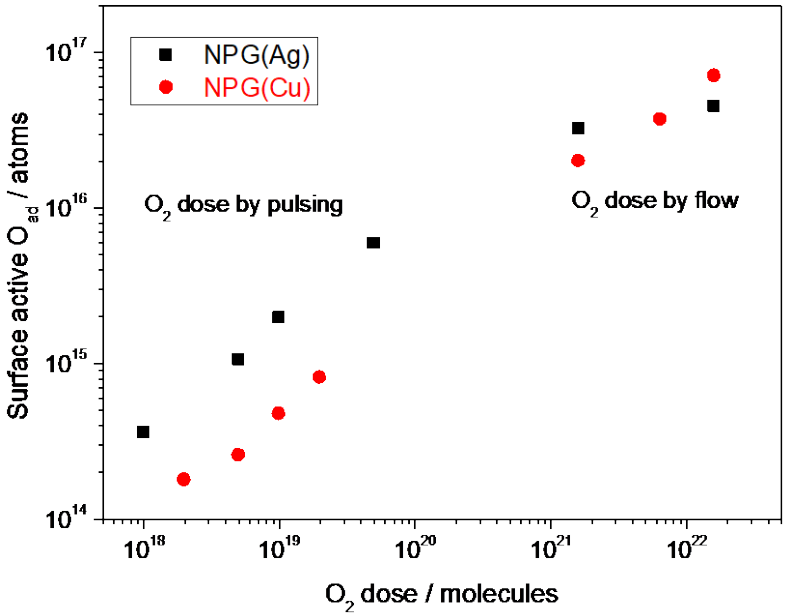

Fig. 5 L.-C. Wang et al.

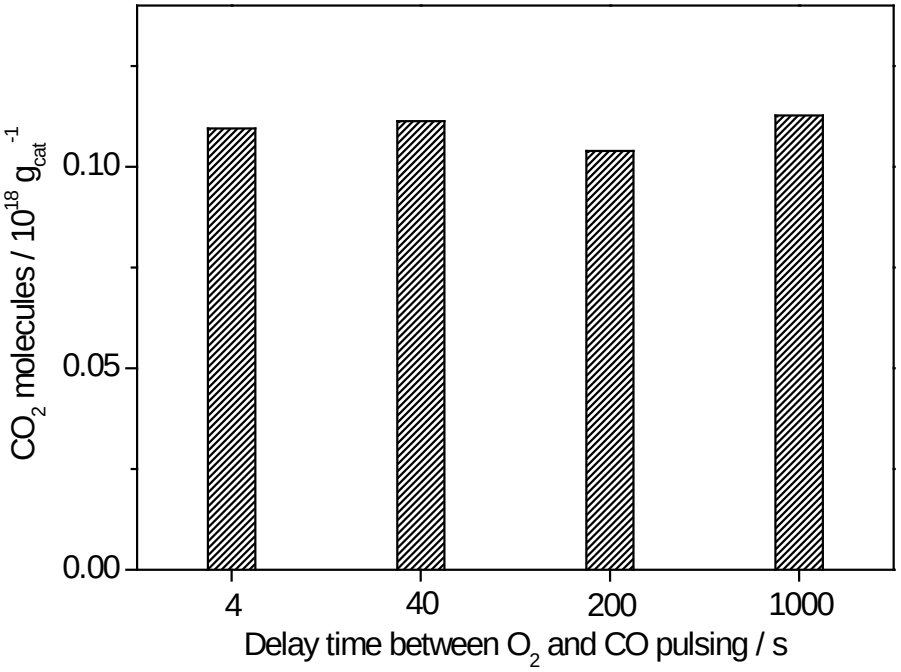

Fig. 6 L.-C. Wang et al.

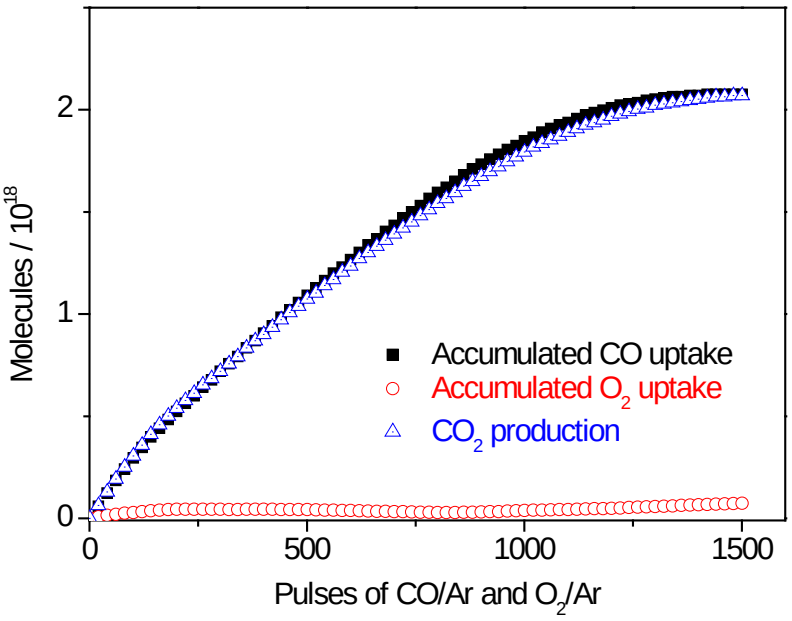

Fig. 7 L.-C. Wang et al.

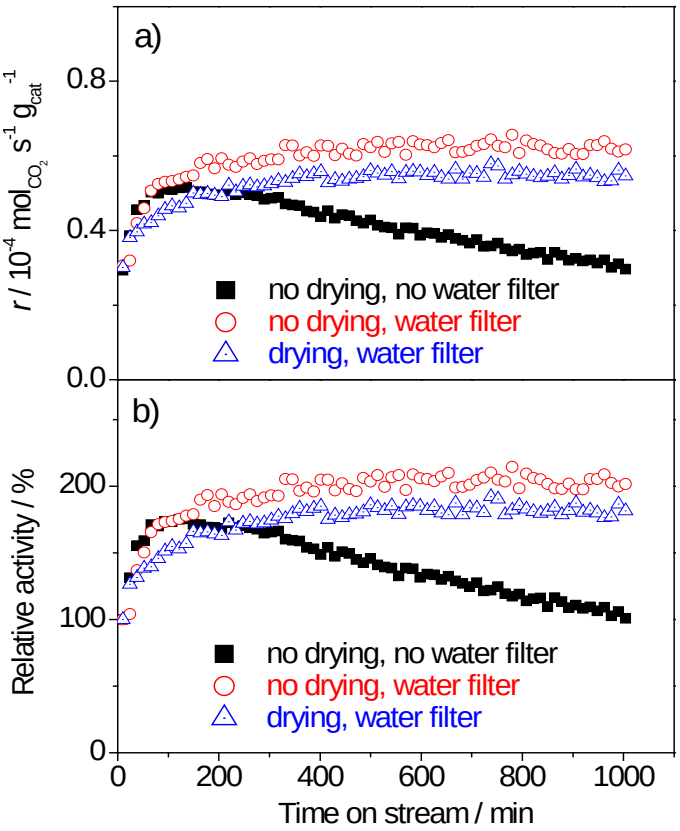

Fig. 8 L.-C. Wang et al.

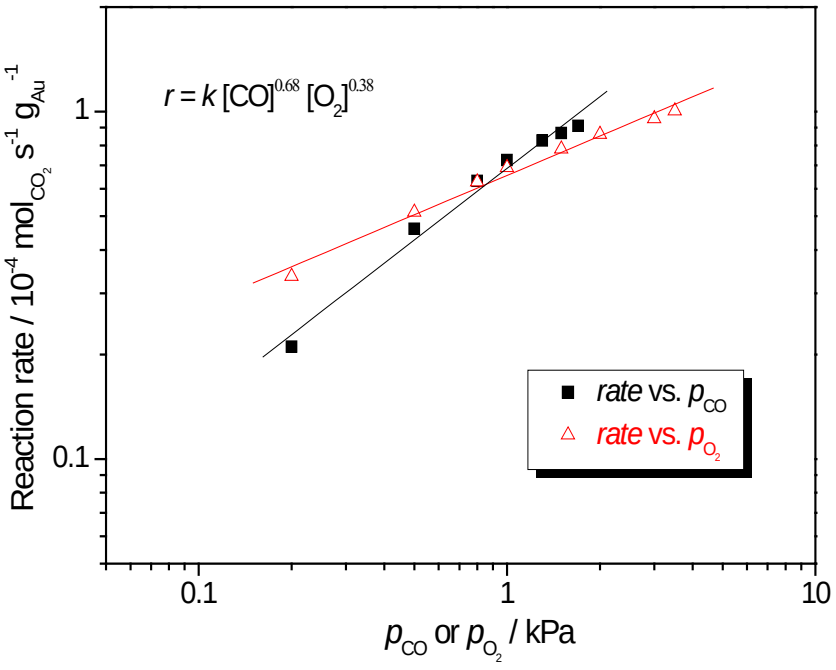

Fig. 9 L.-C. Wang et al.

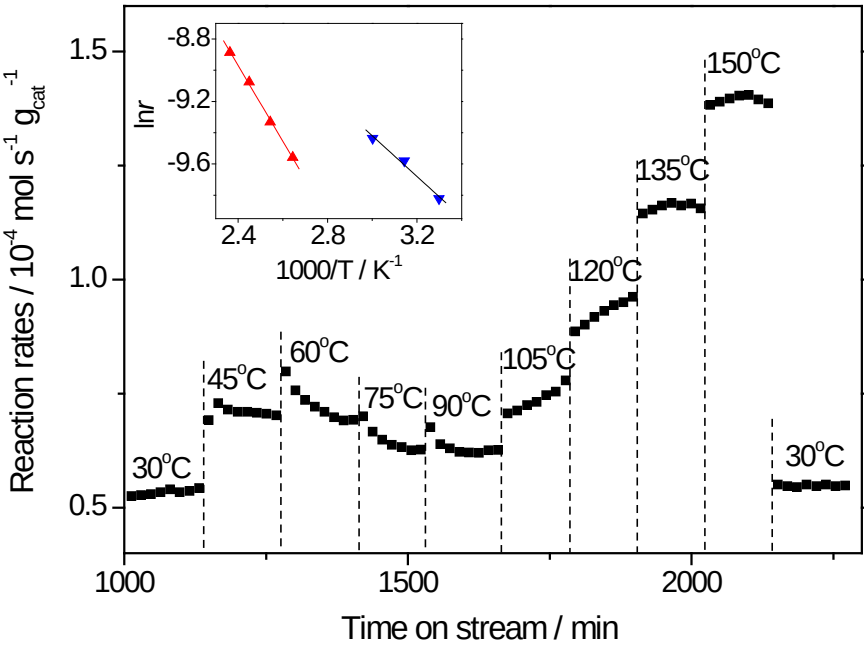

Fig. 10 L.-C. Wang et al.